Neutron decay from the isobaric analog state in ^{120}Sb populated in ^{120}Sn(^{3}He,t)^{120}Sb at $E(^3\text{He}) = 200$ MeV, $\theta = 0°$

D. A. Roberts, K. Ashktorab, F. D. Becchetti, and J. Jänecke
Department of Physics, University of Michigan, Ann Arbor, Michigan 48109

M. N. Harakeh and S. Y. van der Werf
Kernfysisch Versneller Instituut, Zernikelaan 25, 9747 AA Groningen, The Netherlands

G. P. A. Berg, C. C. Foster, J. E. Lisantti, T. Rinckel, E. J. Stephenson, and S. P. Wells
Indiana University Cyclotron Facility, Bloomington, Indiana 47405

A. Nadasen
Department of Natural Sciences, University of Michigan, Dearborn, Michigan 48128

S. Shaheen
King Abdul-Aziz University, Jeddah, Saudi Arabia
(Received 10 April 1995)

The ^{120}Sn(^{3}He,t)^{120}Sb charge-exchange reaction has been investigated at $E(^3\text{He}) = 200$ MeV and $\theta \approx 0°$ to study neutron decay from the isobaric analog state at $E_x = 10.20$ MeV in ^{120}Sb. The low-energy neutrons (average energy ~ 0.85 MeV) were detected in coincidence with tritons observed in the focal plane of a high-resolution magnet spectrometer. Four small deuterated NE230 scintillation detectors were mounted at distances of 9.5 cm from the target resulting in an overall neutron detection efficiency including solid angle of $>1\%$. This efficiency was obtained by combining the measured dependence on neutron energy with a calculated neutron evaporation spectrum. From the measured ratio of coincidence to singles events a branching ratio of $>86\%$ was deduced for neutron decay. The observation of isospin-violating neutron decay with a branching ratio close to 100% is in agreement with the expectation that the escape width ($\Gamma^\uparrow$) of the isobaric analog state in ^{120}Sb is small compared to its spreading width ($\Gamma^\downarrow$). Triton spectra measured in coincidence with γ rays from the deexcitation of the final nucleus display pronounced structures related to the thresholds for neutron emission, in agreement with the characteristics of calculated evaporation spectra.

PACS number(s): 24.30.Gd, 25.55.Kr, 27.60.+j

I. INTRODUCTION

The (p,n) charge-exchange reaction has played an important role in the discovery and study of isobaric analog states (IAS's) and Gamow-Teller resonances (GTR's). Investigations of the (p,n) reaction are complemented by the use of the (^{3}He,t) charge-exchange reaction with its inherently superior energy resolution and higher ejectile detection efficiency. The excellent energy resolution is demonstrated, for example, in a recent investigation [1] of the fragmentation of GTR's and doorway-state substructures. High triton detection efficiencies have been exploited, for example, in numerous studies [2,3] of proton decay from IAS's populated in (^{3}He,t) and the recent studies [4–6] of proton decay from GTR's. The present work reports on the measurement of neutron decay from an IAS's, but the techniques can be extended to the study of giant resonances.

Wave functions for IAS's can be expressed as a sum of a $T_>$ component, obtained by operating with the isospin-lowering operator T^- on the wave function of the parent nucleus, plus a $T_<$ component due to isospin mixing with certain underlying one-particle–one-hole and two-particle–two-hole doorway states. These two components usually lead to direct proton decay and isospin-forbidden statistical neutron decay, respectively [2]. Accordingly, the total width can be written as a sum of an escape and a spreading width, $\Gamma = \Gamma^\uparrow + \Gamma^\downarrow$. The latter is of particular interest because the isospin mixing is believed to be the result of coupling via the Coulomb force to the $(T_0 - 1)$ component of the isovector giant monopole resonance mediated by coupling to doorway states [7–10].

Most experimental spreading widths (compiled for heavier nuclei in Ref. [10]) were obtained indirectly by determining the total widths Γ of IAS's from their Lorentzian line shapes and measuring the branching ratios $P^\uparrow$ for proton decay. The escape and spreading widths become $\Gamma^\uparrow = P^\uparrow\Gamma$ and $\Gamma^\downarrow = P^\downarrow\Gamma = (1 - P^\uparrow)\Gamma$, respectively.

The present work describes an experiment which determines $P^\downarrow$ directly by measuring with a simple geometry but high detection efficiency the neutron decay of an IAS populated preferentially in the (^{3}He,t) charge-exchange reaction near $\theta = 0°$. The isospin-forbidden neutron decay is due to the spreading width $\Gamma^\downarrow$. A similar experiment to determine $\Gamma^\downarrow$ for the isobaric analog state in ^{208}Bi has been reported very recently [11].

II. EXPERIMENTAL PROCEDURES

A. (^{3}He,t) reaction

The experiment was carried out with a 200 MeV $^3\text{He}^{2+}$ beam from the Indiana University Cyclotron Facility (IUCF).

High-resolution triton spectra from the ^{120}Sn(^{3}He,t)^{120}Sb charge-exchange reaction were obtained by magnetic analysis using the K600 magnetic spectrometer [12,13]. The measurements were carried out near $\theta=0°$, and the $^3He^{2+}$ beam particles, which also enter the spectrometer, were deflected inward and stopped in an electrically insulated beam stop. Details of the experimental setup, including the magnetic spectrometer and the focal-plane detection system, are given in Refs. [3,14,1].

An isotopically enriched ^{120}Sn target of thickness $\rho\Delta x=9.7$ mg/cm^2 was used, and the beam current was typically ~ 7 e nA. Singles events were prescaled by a ratio of 10:1 before writing to tape to reduce dead time and to optimize the coincidence rate with neutrons.

The ray-tracing capabilities of the focal-plane detection system make it possible to decompose the measured triton spectra into two separate spectra for angles centered near $\theta\approx 0°$ and $\theta\approx 2°$, respectively. This provides a signature for $\Delta L=0$ transitions which are strongly peaked at $\theta=0°$. The angular distribution for the (^{3}He,t) transition to the IAS in ^{120}Sb was observed [3] to display strong oscillations with the first minimum at $\theta\approx 3°$.

B. Neutron detectors

In order to measure triton spectra correlated with evaporation neutrons from the decay of excited states and resonances in the final nucleus, neutrons have to be detected in coincidence with the tritons. The setup consisted of four small NE230 liquid scintillators (2 in. diameter $\times$2 in. thickness) mounted very close to the target at distances of 9.5 cm and at angles of 135° with respect to the beam direction. Two additional NE213 liquid scintillators (5 in. diameter $\times$5 in. thickness) were mounted at distances of 29.5 cm from the target at angles of $\pm 90°$. However, only one of these two detectors yielded useful neutron decay data because the second detector was in the line of sight from the beam stop inside the first dipole magnet which resulted in a high background.

NE230 is a fully deuterated liquid scintillator material [15] which has a response function with a maximum at the highest deuteron recoil energy. This makes it useful for measurements at higher neutron energies where low- to medium-resolution neutron spectra can be obtained directly without the need for time-of-flight information [16]. The neutron detection efficiency for NE230 is somewhat lower than that for NE213.

Time of flight and pulse-shape discrimination were employed to separate neutron and γ-ray events. Despite the short flight path, time of flight was useful to identify slow neutrons where pulse-shape discrimination is less effective. Neutrons and γ rays were detected in coincidence with several beam bursts (rf) gated on focal-plane events. This allowed the identification of prompt and random events. The prompt events in the present experiment were composed of about 30% random and 70% true coincidences. Coincidence spectra used for the analysis were obtained by gating on true events defined as prompt minus random events.

C. Neutron-detector calibration

The pulse-height spectra for the neutron detectors were calibrated using the Compton edges of γ rays from ^{22}Na and other calibration sources. The thresholds in the present experiment were set at $E_e^{\rm thr}\approx 28$ keVee (ee=electron equivalent) which corresponds to a neutron energy threshold of $E_n^{\rm thr}\approx 350$ keV. Special attention was given to achieving such low pulse-height thresholds because the emitted neutrons have low energies ($E_n<3200$ keV) with a maximum in the evaporation spectrum at $E_n\approx 450$ keV and an average energy of $E_n\approx 850$ keV.

The detection efficiencies of the neutron detectors were determined with a calibrated ^{252}Cf fission source. Coincidences between fission fragments detected with a xenon gas scintillation detector and neutrons from this source were observed, and the energies of the neutrons were selected by their time of flight over a flight path of 1 m. The neutron spectrum from ^{252}Cf has a well-known shape [17] which allows an absolute determination of the detection efficiencies in the energy range 0.5–10 MeV. Selecting slices in the two-dimensional pulse-height versus time-of-flight spectra, pulse-height distributions were obtained for neutron energies in steps of 0.5–1 MeV. The energy dependence of the neutron detection efficiencies η_n was obtained from these distributions for several hardware and software thresholds. A set of detection efficiencies for the small 2 in. thick NE230 liquid scintillators is displayed in Fig. 1 for three different thresholds in the range from $E_e^{\rm thr}\approx 30$ to 500 keVee. This corresponds to neutron energy thresholds from $E_n^{\rm thr}\approx 350$ to 2400 keV (see figure caption). Curve (a) was obtained with a hardware threshold. The data will be discussed in more detail in Sec. IV A.

III. EXPERIMENTAL RESULTS

Figure 2(a) displays a triton spectrum measured in singles mode with the magnetic spectrometer covering angles $\theta\leq 3°$. A second overlapping spectrum measured indepen-

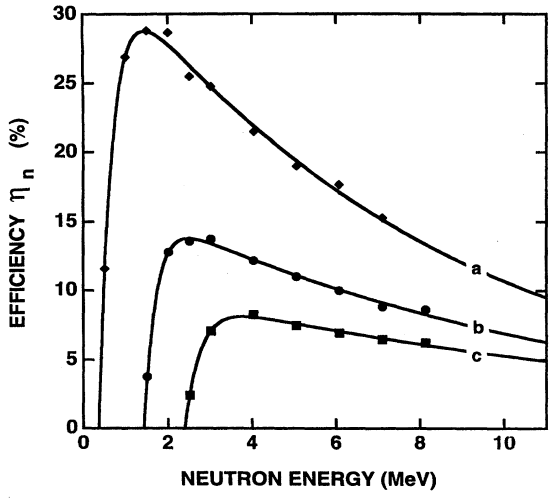

FIG. 1. Neutron detection efficiencies obtained with a ^{252}Cf source as function of the neutron energy for a NE230 liquid scintillator (2 in. diameter $\times$2 in.). The detection thresholds $E_e^{\rm thr}$ ($E_n^{\rm thr}$) are (a) 29 keVee (354 keV), (b) 204 keVee (1425 keV), (c) 502 keVee (2396 keV). The solid lines are included to guide the eye.

dently for higher excitation energies is not shown. The singles events were prescaled by the ratio 10:1 to reduce computer dead time and in doing so to allow the collection of coincidence events with higher beam currents. The most obvious feature of the spectrum of Fig. 2(a) is the strong transition to the 0^+ IAS in ^{120}Sb at $E_x = 10.20$ MeV. Selective transitions to the 1^+ ground state in ^{120}Sb and a few other low-lying states can also be seen. Furthermore, two broad resonances are superimposed on a nonresonant background.

The decomposition by ray tracing of this spectrum into spectra for angles of $\theta \approx 0°$ and $\theta \approx 2°$ (see Figs. 2 and 3 in Ref. [14] or Fig. 2 in Ref. [1]) provides a clear signature for $\Delta L = 0$ transitions with the strong enhancement at $\theta = 0°$. These features become most prominent in the difference spectra for $\theta \approx 0°$ and $\theta \approx 2°$. This decomposition is not necessary in the present IAS work, but it was particularly important for identifying the GTR at $E_x \approx 11.5$ MeV and low-lying Gamow-Teller fragments. The charge-exchange giant resonance at $E_x \approx$ 19.6 MeV displays a minimum at $\theta = 0°$ which is characteristic for $\Delta L = 1$. Investigations of these resonances have been reported for ^{117,120}Sn(^{3}He,t)^{117,120}Sb [3] and subsequently for all stable Sn targets [1]. The decomposition of all spectra into a nonresonant background and charge-exchange giant resonances, particularly the GTR's with their low-lying fragments and the appearance of doorway states, has been discussed in detail elsewhere [1].

Figure 2(b) displays the triton spectrum which was measured simultaneously with the singles spectrum of Fig. 2(a) at angles near $\theta = 0°$ in true coincidence with neutrons. The neutrons were detected in the five neutron detectors with an average hardware threshold of $E_e^{\text{thr}} \approx 28$ keVee. The spectrum displays an onset at about $E_x \approx 7$ MeV due to the threshold for neutron emission in ^{120}Sb at $E_x = 7.019$ MeV. The few counts observed below this threshold are from γ rays which are not completely removed by pulse-shape discrimination in the difference of prompt minus random events. The IAS is again very dominant, and the two broad resonances are identified as Gamow-Teller and $\Delta L = 1$ resonances, respectively. As expected, even without the decomposition into $\theta \approx 0°$ and $\theta \approx 2°$ spectra, the relative contribution from a nonresonant background is reduced compared to that in the singles spectrum of Fig. 2(a), and the giant resonances are more prominent.

The number of singles events recorded for the IAS in the spectrum of Fig. 2(a) multiplied by the prescaling factor is $N_s = 146\,155 \pm 2089$. The corresponding number of coincidence events recorded with the four NE230 neutron detectors is $N_c = 2148 \pm 100$. Since, as mentioned above and seen in Fig. 2(b), pulse-shape discrimination did not completely remove all γ-ray events, a reduction of the number of coincidence events by 5% was considered necessary. This leads to a slightly corrected value of $N_c = 2041 \pm 113$. The ratio of the two numbers is $N_c/N_s = 0.014 \pm 0.001$. Anticipating a branching ratio for neutron decay from the IAS of close to 100%, this implies a total detection efficiency for evaporation neutrons of $>1\%$.

Figure 2(c) displays a triton spectrum measured in coincidence with γ rays from the NE230 detectors with a threshold of ~ 65 keVee. In addition to the IAS, the spectrum shows pronounced structures which appear to be unrelated to those seen in Figs. 2(a) and 2(b). These features will be discussed in Sec. IV C.

IV. DISCUSSION

A. Neutron detection efficiencies

The determination of the experimental branching ratio for neutron decay from the IAS requires the knowledge of the shape of the neutron spectrum and the efficiency for the detection of neutrons with its dependence on energy as discussed in Sec. II C.

A calculated neutron evaporation spectrum from the statistical decay of the 0^+ IAS in ^{120}Sb to states in ^{119}Sb is displayed in Fig. 3. The spectrum is normalized to 1000 decays. It was obtained with the computer code CASCADE [18]

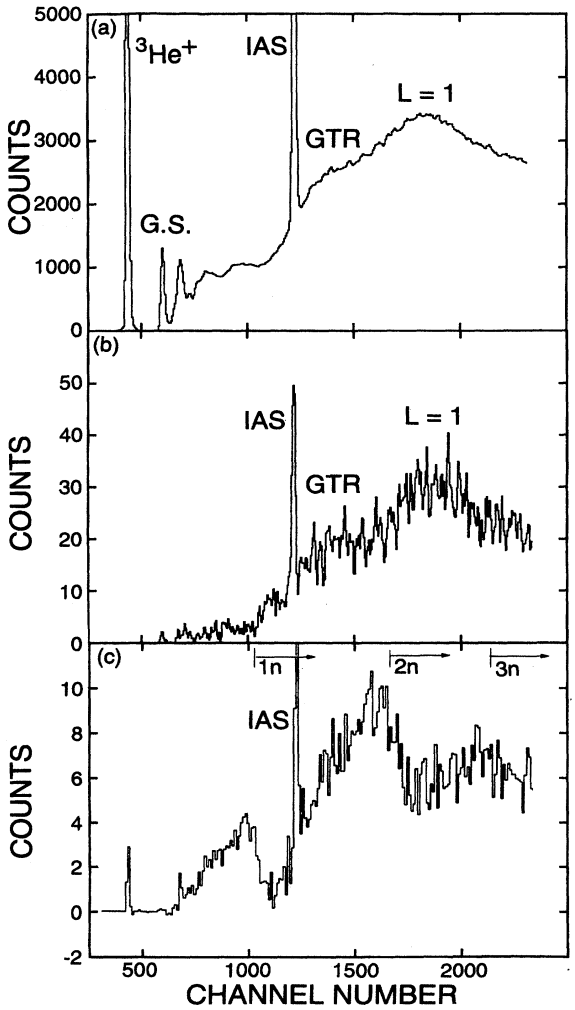

FIG. 2. Triton energy spectra from the ^{120}Sn(^{3}He,t)^{120}Sb reaction at $E(^3\text{He}) = 200$ MeV and $\theta < 3°$ for excitation energies up to $E_x = 25$ MeV. (a) Triton energy spectrum measured in singles mode. (b) Triton energy spectrum measured in coincidence with evaporation neutrons of energy >350 keV and gated on true = prompt − random events. (c) Triton energy spectrum measured in coincidence with γ rays of energy >65 keV and gated on true = prompt − random events.

which takes into consideration the statistical decay into the final states described by the backshifted Fermi-gas model [19] and appropriate level-density parameters as well as the parameters for the giant dipole strength. Several low-lying states are included explicitly. Isospin selection rules were not invoked, and the neutron decay is assumed to originate from the $T_<$ component of the IAS wave function. The calculated total number of neutrons is 0.989/decay with only weak competition from the emission of primary gamma rays (0.010/decay) and protons (0.001/decay). Sequential neutron decay from states populated in ^{119}Sb is energetically not possible. Direct neutron decay is usually negligible. On the other hand, direct proton decay (which is due to the escape width $\Gamma^{\uparrow}$) often competes in intensity with the statistical neutron decay (which is due to the spreading width $\Gamma^{\downarrow}$).

The calculated neutron spectrum shown in Fig. 3 displays a linear increase at low energies. This reflects upon the energy dependence of the transmission coefficient. It is followed by a maximum at $E_n \approx 450$ keV and a subsequent decrease due to the decrease in the density of final states. Discrete contributions at energies above 1.5 MeV up to 3.2 MeV are the result of statistical decays to the ground and discrete low-lying states in ^{119}Sb.

The integrated neutron spectrum

$$I_0(E_e^{\rm thr}) = \int_{E_n^{\rm thr}}^{\infty} S_n(E_n)\, dE_n , \tag{1}$$

expressed as function of the threshold $E_e^{\rm thr}$, represents the fraction of the spectrum above this threshold. For $E_e^{\rm thr}=30$, 100, and 250 keVee, the detectors are only sensitive to $\sim 70\%$, $\sim 35\%$, and $\sim 10\%$ of the full spectrum. When the detector efficiencies used in the present experiment are included (see below), the neutrons from the evaporation spectrum are recorded with efficiencies of only $\sim 18\%$, $\sim 4\%$, and $\sim 0.5\%$, respectively, numbers which have to be multiplied further by the relative solid angle. Clearly, the shape of the distribution of evaporation neutrons with its low maximum energy of 3.2 MeV demonstrates the need for a very low neutron energy detection threshold below 0.5 MeV.

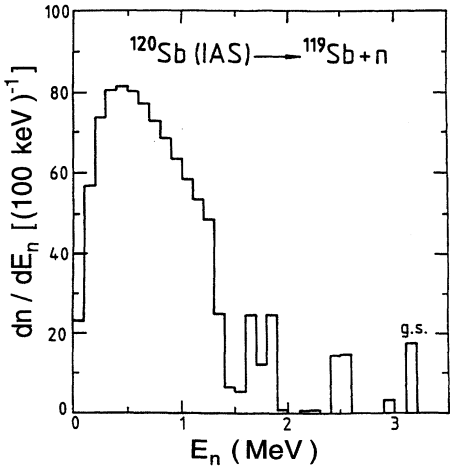

FIG. 3. Calculated energy spectrum for evaporation neutrons from the statistical decay of the 0^+ IAS in ^{120}Sb to states in ^{119}Sb.

Determining the integral efficiency for the detection of neutrons with an energy spectrum as given by Fig. 3 requires knowledge of the energy dependence of the neutron detection efficiency $\eta_n(E_e^{\rm thr},E_n)$ for the threshold of $E_e^{\rm thr}\approx 28$ keVee used in the present experiment. Absolute neutron detection efficiencies determined from the ^{252}Cf calibration data are shown in Fig. 1 for three hardware and/or software thresholds ranging from $E_e^{\rm thr}\approx 29$ to 502 keVee with corresponding neutron energy thresholds from $E_n^{\rm thr}\approx$ 0.35 to 2.40 MeV. The thresholds were determined directly from the measured data. They are in agreement with the light output reported for electrons and deuterons in Ref. [15]. The neutron detection efficiencies reach a maximum value of $\sim 29\%$ for the lowest threshold setting of $E_e^{\rm thr}\approx 29$ keVee and are expected to be a little higher when extrapolated to $E_e^{\rm thr}\approx 28$ keVee.

The integrated detection efficiencies defined as

$$I(E_e^{\rm thr}) = \int_{E_n^{\rm thr}}^{\infty} \eta_n(E_e^{\rm thr},E_n) S_n(E_n)\, dE_n \tag{2}$$

have been obtained for six detector thresholds $E_e^{\rm thr}$ by integrating the calculated neutron spectrum S_n of Fig. 3 folded with the absolute neutron detection efficiencies η_n of Fig. 1 and another set of three measurements. The values follow an approximate power-law dependence. They can reliably be extrapolated to the threshold used in the present experiment yielding

$$I(28\ \text{keVee}) = (18.9 \pm 2.1)\%. \tag{3}$$

An uncertainty of 11% was assigned to this value based on the uncertainties of the thresholds, the absolute fission rates determined in the ^{252}Cf measurement, and possible uncertainties in the calculated evaporation spectrum. The main uncertainty results from the value of $I(29$ keVee) because of the strong dependence on the threshold $E_e^{\rm thr}$. An uncertainty of only ± 2 keVee in the threshold is responsible for a $\pm 11\%$ uncertainty in $I(E_e^{\rm thr})$. The uncertainty in $E_e^{\rm thr}$ is in part due to the poor pulse height resolution at low neutron energies.

It was observed that the slightly different thresholds used in the (^{3}He,tn) experiment for the four NE230 detectors had the expected effect on the observed coincidence rates, and similar uncertainties must therefore apply to these threshold energies. Uncertainties of $\pm 11\%$ were therefore folded into the uncertainties for the number of coincidence events, N_c.

Calculations with Monte Carlo simulation codes have also been performed to determine the absolute neutron detection efficiencies η_n for liquid NE230 scintillators. Existing codes [20,21] were generalized by including neutron-deuteron interactions and the light-output function for the recoiling deuterons. Moderate agreement with the experimental values has been achieved.

Combining the integral detection efficiency of $I(28$ keVee)$=(18.9\pm 2.1)\%$ for evaporation neutrons with the relative solid angle for the four small NE230 detectors yields an absolute detection efficiency of

$$\epsilon=(1.35\pm0.15)\%. \quad (4)$$

This value is somewhat increased when the contributions from the fifth large-volume detector (with the known properties of the NE213 scintillation liquid) at the larger distance of 29.5 cm are included. However, the increased uncertainties introduced with this detector did not justify its inclusion, confirming the advantage of using small detectors very close to the target.

B. Spreading width $\Gamma^{\downarrow}$ of the IAS

Combining the recorded numbers of singles and neutron coincidence events for the IAS, N_s and N_c from Sec. III, with the absolute detection efficiency ϵ from the previous section yields a branching ratio for the emission of neutrons of

$$P^{\downarrow}=\Gamma^{\downarrow}/\Gamma\approx\Gamma_n/\Gamma=(103\pm17)\%>86\%. \quad (5)$$

Here, the uncertainties of the numbers of events, N_s and N_c, were combined with the uncertainties due to the thresholds in the ^{252}Cf measurements and the actual coincidence measurements. The spreading width $\Gamma^{\downarrow}$ follows directly from this ratio and the known experimental total width $\Gamma=32\pm9$ keV for the IAS in ^{120}Sb [22]. The result is $\Gamma^{\downarrow}=P^{\downarrow}\Gamma=33.0\pm10.8$ keV. The above values are included in Table I together with calculated values from Refs. [10,23].

The calculated width of about 30 keV shown in the table is part of a general trend established for the spreading widths $\Gamma^{\downarrow}$ of 65 nuclei with $A\geq110$ based on coupling of the IAS with the isovector giant monopole resonance. These theoretical estimates [10] represent global trends, and they are not expected to give good agreement for individual nuclei. Nevertheless, the agreement for the IAS in ^{120}Sb is very good. It should also be noted that the calculations of Ref. [10] describe quite well the relatively small and constant values of $\Gamma^{\downarrow}$ for the entire Sn region [23], and they describe the strong increase of $\Gamma^{\downarrow}$ with neutron excess for many deformed rare-earth nuclei. It appears, though, that some disagreement may exist in the trends observed [24] for nuclei slightly lighter than ^{208}Pb and the predictions from Ref. [10]. However, this region includes nuclei with triaxial shapes and negative deformations where the equations of Ref. [10] may not apply.

A more precise indirect estimate of $\Gamma^{\downarrow}$ for the IAS in ^{120}Sb has been obtained recently [23] by employing a procedure outlined in Ref. [25]. Absolute values of the escape widths $\Gamma^{\uparrow}$ were obtained for the IAS's of all Sn and Te isotopes [23] using calculated single-particle escape widths and experimental spectroscopic factors measured in single-neutron pickup reactions such as (p,d) or (d,t) on the respective target nuclei. These values were found to be in very good agreement with existing data. They display a pronounced odd-A–even-A staggering effect, with branching ratios $P^{\uparrow}$ for direct proton decay of only a few percent for the IAS's of all even-A Sn and Te isotopes. Spreading widths were then derived indirectly from $\Gamma^{\downarrow}=\Gamma-\Gamma^{\uparrow}$. Most of the total widths Γ for Sn and Te isotopes are from the experimental work of Becchetti *et al.* [22] who measured Γ in the (^{3}He,t) charge-exchange reaction for essentially all stable Sn and Te isotopes. The deduced branching ratio $P^{\downarrow}$ of (95.9 $\pm$2.3)% for the IAS of ^{120}Sn is included in Table I.

TABLE I. Experimental and calculated branching ratios $P^{\downarrow}$ and spreading widths $\Gamma^{\downarrow}$ for neutron decay of the IAS in ^{120}Sb with $\Gamma^{\downarrow}=P^{\downarrow}\Gamma$ and $\Gamma=32\pm9$ keV from Ref. [22].

	$P^{\downarrow}$	$\Gamma^{\downarrow}$
Experimental (this work)	>86%	33.0$\pm$10.8 keV
Calculated [10]	~90%	~30 keV
Calculated [23]	95.9$\pm$2.3%	30.7$\pm$8.7 keV

A branching ratio of close to 100% for an isospin-forbidden neutron decay is unusual. This is because the isospin-allowed direct proton decay with its relatively low maximum decay energy of $E_p=4.60$ MeV is strongly suppressed due to the Coulomb barrier. This leads to a low single-particle escape width of only 1.74 keV. However, $\Gamma^{\downarrow}$ and $P^{\downarrow}$ are not related to transition probabilities for neutron decay [23]. Instead, they are related to the "spreading" of the pure IAS wave function, obtained by operating with the isospin-lowering operator T^- on the parent state, into the doorway states. The time evolution of this "spreading" takes place on a scale of 10^{-19} s. It depends on the charge-dependent matrix element V_{CD} for mixing between the IAS and the $T_<$ component of the isovector giant monopole resonance (IVGMR), on the density of one-particle–one-hole and two-particle–two-hole doorway states, and on the nuclear matrix elements connecting the IVGMR and the doorway states. Subsequent neutron decay from the doorway states is slow and sequential, and it usually does not affect the width. In fact, neutron decay is energetically not even possible for the decay of the IAS of ^{114}Sn, for example, and "spreading" is followed here by gamma decay instead on an even slower time scale.

C. Neutron and γ-ray coincidence spectra

Figures 2(b) and 2(c) show triton spectra measured in the focal-plane detectors in coincidence with neutrons and γ rays, respectively. The detector thresholds for neutrons and γ rays are $E_n^{\rm thr}\approx350$ keV (or $E_e^{\rm thr}\approx28$ keVee) and $E_\gamma^{\rm thr}\approx65$ keV (or $E_e^{\rm thr}\approx65$ keVee), respectively. Whereas both spectra display the IAS quite strongly, the structure of the continuum differs significantly. The neutron-gated spectrum [Fig. 2(b)] shows the threshold for neutron emission and, as mentioned before, the Gamow-Teller and $\Delta L=1$ resonances are more pronounced than in the singles spectrum. This is due to the fact that the nonresonant background from quasifree charge exchange leaves the residual nucleus at lower excitation energies and hence leads to reduced neutron emission.

The spectrum of Fig. 2(c) measured in coincidence with γ rays has entirely different characteristics seemingly unrelated to that of Fig. 2(b). The observed broad structures are not related to any known giant resonances. Instead, they are closely connected with the thresholds for neutron emission. Below the threshold for the emission of a single neutron, the yield for γ emission increases strongly but drops sharply to essentially zero at the neutron threshold. A similar situation occurs at the threshold for the emission of two and three neutrons, but the effect is less pronounced. Data for higher excitation energies (not shown) still show this effect weakly

at the thresholds for the emission of four and five neutrons.

The behavior observed in Figs. 2(b) and 2(c) is a natural consequence of the competing decay modes, and it can be described with the statistical-model code CASCADE [18]. Figure 4 displays the calculated number of neutrons and γ rays emitted above certain assumed thresholds as function of the excitation energy in the nucleus ^{120}Sb. Decays from 0^+ states are assumed, but decays from states with other J^π will basically show the same characteristics. At very low neutron-detector thresholds, the response increases in unit steps at each new neutron threshold, i.e., (^{3}He,tn), (^{3}He,$t2n$), (^{3}He,$t3n$). However, these steps are smoothed out when the neutron detection thresholds are increased. This increase in neutron multiplicity increases the efficiency with which highly excited giant resonances, such as the isovector giant monopole resonance, can be detected in coincidence with decay neutrons.

In contrast, the calculations for γ emission display completely different structures related to the thresholds for neutron emission. Following the initial increase in the number of gamma rays below the first neutron threshold, a sharp decrease is indeed predicted at this threshold due to competition with neutron emission. Interestingly, the minimum is essentially zero, independent of the detector threshold. The yield increases again with increasing excitation energy, leading to a maximum at the emission of two neutrons followed by a strong decrease. Similar maxima and minima are predicted at the higher thresholds, but the structures become less pronounced with increasing energy and increasing detector threshold due to the increasing overlap in phase space of multineutron decay. It follows from these calculations that one has to be very careful when measuring ejectile spectra in coincidence with γ rays to avoid spurious features due to threshold effects.

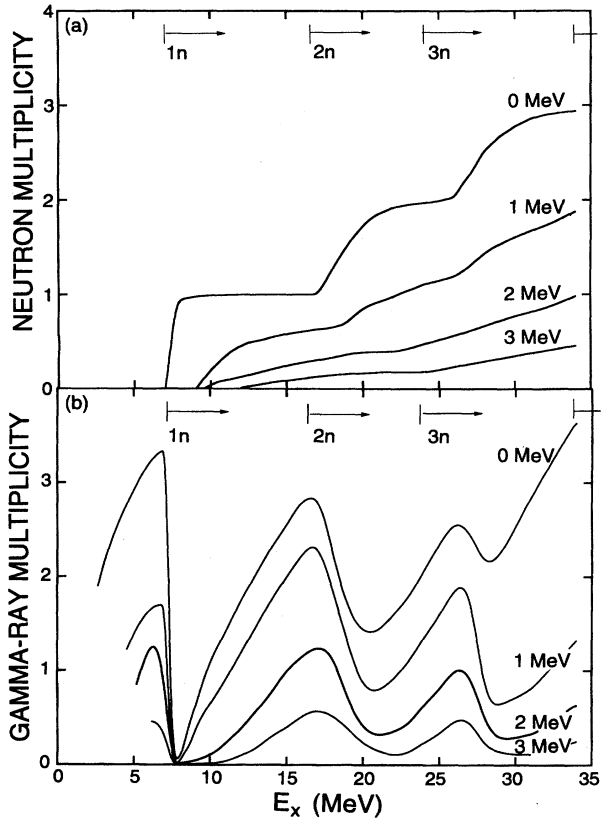

FIG. 4. Multiplicities for the emission of neutrons and γ rays as function of excitation energy in the nucleus ^{120}Sb obtained with the statistical-model code CASCADE [18]. The respective sets of curves are obtained for different detector threshold energies as indicated.

D. General comments

Improved measurements of triton spectra in coincidence with neutron decay yielding the spreading widths $\Gamma^\downarrow$ of IAS's, as described in the present work, and enhancing the structures of Gamow-Teller and other high-lying resonances with respect to the underlying continuum, are possible and desirable. This can be achieved using a few small detectors close to the target as was done in the present experiment. Using more than four 2 in. NE230 (or alternatively NE213) detectors will result in increased coincidence count rates and improved statistics. Alternatively, the use of a large "neutron wall" at a distance of typically 2 m from the target, as was done in the investigation of the neutron decay of the IAS in ^{208}Bi [11], makes neutron time-of-flight measurements possible. This has the advantage that evaporation spectra can be measured. The total neutron detection efficiencies of typically 2% are similar for the two techniques.

Problems due to the sensitivity of the absolute neutron detection efficiencies for low detector thresholds, as experienced in the present work, are common to both techniques. The need for low thresholds depends on the neutron separation energy and the excitation energy of the decaying state or resonance which determine the maximum energy in the neutron evaporation spectrum, e.g., $E_n^{\max}=3.1$ MeV for the decay of the IAS in ^{120}Sb, but $E_n^{\max}=8.3$ MeV for the corresponding decay of the IAS in ^{208}Bi [11]. Obviously, the present techniques cannot be employed when the maximum neutron energies are low as, for example, for the decays of the IAS's of ^{116,117}Sn (0.49 and 1.38 MeV, respectively). Neutron decay is not even permitted from the IAS's of the lighter ^{114,115}Sn isotopes but replaced by statistical proton decay or γ-ray emission. On the other hand, the maximum neutron energies are increased for the studies of the decays of high-lying giant resonances with the added advantage, as outlined in Sec. IV C, of increased neutron multiplicity.

V. SUMMARY

Neutron decay from the IAS in ^{120}Sb has been measured, and the branching ratio for this isospin-forbidden decay mode was observed to be close to 100% in agreement with predictions for the escape and spreading widths, $\Gamma^\uparrow$ and $\Gamma^\downarrow$, respectively. The IAS was excited in the (^{3}He,t) charge-exchange reaction at $E(^3\text{He})=200$ MeV and $\theta\approx 0°$. The neutrons were detected with four small deuterated NE230 liquid scintillators mounted close to the target. The neutron detection efficiencies were determined with neutrons from a ^{252}Cf source by measuring coincidences between fission fragments and neutrons. The general shapes of triton spectra measured in coincidence with neutrons and with γ rays show

a different behavior which can be explained using calculated evaporation spectra on the basis of competition between the two decay modes.

ACKNOWLEDGMENTS

The authors acknowledge the support by the technical staff at IUCF and the help provided by W. R. Lozowski. We also thank Kristin Dennis, M. Dwueke, D. P. Stewart, S. Yeh, and J. E. Elek for their help with data reduction. Thanks are due to G. F. Knoll for making available to us the ^{252}Cf fission source and the xenon gas scintillation counter used in the calibration of the neutron detectors. The research was supported in part by the National Science Foundation Grants Nos. PHY-9208468 with REU supplements (UM, Ann Arbor), PHY-9312428 (UM, Dearborn), and PHY-9314783 (IUCF). Travel support by the Scientific Affairs Division, North Atlantic Treaty Organization, travel Grants Nos. NATO 85-0123 and 90-0219 is gratefully acknowledged.

[1] K. Pham, J. Jänecke, D. A. Roberts, M. N. Harakeh, G. P. A. Berg, S. Chang, J. Liu, E. J. Stephenson, B. Davis, H. Akimune, and M. Fujiwara, Phys. Rev. C **51**, 526 (1995); J. Jänecke *et al.*, in International Conference on Selected Topics in Nuclear Structure, Dubna, Russia, 1994, Report No. JINR E4-94-370, 1994, p. 29.

[2] H. J. Hofmann, S. Brandenburg, P. Grasdijk, M. N. Harakeh, W. A. Sterrenburg, and S. Y. van der Werf, Nucl. Phys. **A433**, 181 (1985), and references therein.

[3] J. Jänecke, F. D. Becchetti, A. M. van den Berg, G. P. A. Berg, G. Brower, M. B. Greenfield, M. N. Harakeh, M. A. Hofstee, A. Nadasen, D. A. Roberts, R. Sawafta, J. M. Schippers, E. J. Stephenson, D. P. Stewart, and S. Y. van de Werf, Nucl. Phys. **A526**, 1 (1991).

[4] H. Akimune, I. Daito, Y. Fujita, M. Fujiwara, M. B. Greenfield, M. N. Harakeh, T. Inomata, J. Jänecke, K. Katori, S. Nakayama, H. Sakai, Y. Sakemi, M. Tanaka, and M. Yosoi, Phys. Lett. B **323**, 107 (1994).

[5] H. Akimune, I. Daito, Y. Fujita, M. Fujiwara, M. B. Greenfield, M. N. Harakeh, T. Inomata, J. Jänecke, K. Katori, S. Nakayama, H. Sakai, Y. Sakemi, M. Tanaka, and M. Yosoi, Nucl. Phys. **A569**, 255c (1994).

[6] M. N. Harakeh, H. Akimune, I. Daito, Y. Fujita, M. Fujiwara, M. B. Greenfield, T. Inomata, J. Jänecke, K. Katori, S. Nakayama, H. Sakai, Y. Sakemi, M. Tanaka, and M. Yosoi, Nucl. Phys. **A577**, 51c (1994).

[7] A. Z. Mekjian, Nucl. Phys. **A146**, 288 (1970).

[8] N. Auerbach, J. Hüfner, A. K. Kerman, and C. M. Shakin, Rev. Mod. Phys. **44**, 48 (1972).

[9] W. M. MacDonald and M. C. Birse, Phys. Rev. C **29**, 425 (1984).

[10] J. Jänecke, M. N. Harakeh, and S. Y. van der Werf, Nucl. Phys. **A463**, 571 (1987).

[11] J. A. Bordewijk, A. Balanda, D. Beaumel, J. Blomgren, S. Brandenburg, G. van 't Hof, M. N. Harakeh, M. A. Hofstee, J. Jänecke, A. Krasznahorkay, H. Laurent, L. Nilsson, N. Olsson, R. Perrino, R. Siebelink, P. O. Söderman, S. Y. van der Werf, and A. van der Woude, Nucl. Phys. **A574**, 453 (1994).

[12] G. P. A. Berg, L. C. Bland, B. M. Cox, D. DuPlantis, D. W. Miller, K. Murphy, P. Schwandt, K. A. Solberg, E. J. Stephenson, B. Flanders, and H. Seifert, IUCF scientific and technical report, 1986 (unpublished), p. 152.

[13] G. P. A. Berg, L. C. Bland, D. DuPlantis, C. C. Forster, D. W. Miller, P. Schwandt, R. Sawafta, K. A. Solberg, and E. J. Stephenson, IUCF scientific and technical report, 1987-1988 (unpublished), p. 233.

[14] J. Jänecke, K. Pham, D. A. Roberts, D. Stewart, M. N. Harakeh, G. P. A. Berg, C. C. Foster, J. E. Lisantti, R. Sawafta, E. J. Stephenson, A. M. van den Berg, S. Y. van der Werf, S. E. Muraviev, and M. H. Urin, Phys. Rev. C **48**, 2828 (1993).

[15] D. L. Smith, R. G. Polk, and T. G. Miller, Nucl. Instrum. Methods **64**, 157 (1968); R. L. Craun and D. L. Smith, *ibid.* **80**, 239 (1970).

[16] D. A. Roberts, F. D. Becchetti, K. Ashktorab, D. Stewart, J. W. Jänecke, H. R. Gustafson, and M. J. Dueweke, IEEE Trans. Nucl. Sci. **NS-39/4**, 532 (1992).

[17] J. Cub, E. Finkh, K. Gebhardt, K. Geissdorfer, R. Lin, J. Strate, and H. Klein, Nucl. Instrum. Methods A **274**, 217 (1989).

[18] F. Pühlhofer, Nucl. Phys. **A280**, 267 (1977); M. N. Harakeh (unpublished).

[19] W. Dilg, W. Schantl, H. Vonach, and M. Uhl, Nucl. Phys. **A217**, 269 (1973).

[20] R. A. Cecil, B. D. Anderson, and R. Madey, Nucl. Instrum. Methods **161**, 439 (1979).

[21] G. Dietze and H. Klein, Monte Carlo Code NEFF4, Report No. ISSN 0572-7170, Bericht PTB-ND-22, Braunschweig, 1982.

[22] F. D. Becchetti, W. S. Gray, J. Jänecke, E. R. Sugarbaker, and R. S. Tickle, Nucl. Phys. **A271**, 77 (1976).

[23] J. Jänecke, J. A. Bordewijk, S. Y. van der Werf, and M. N. Harakeh, Nucl. Phys. **A552**, 323 (1993).

[24] S. Y. van der Werf, in Proceedings of the 6th International Conference on Nuclear Excitations and Mechanisms, edited by E. Gadioli, Varenna, Italy, 1991 (unpublished), p. 530.

[25] S. Y. van der Werf, M. N. Harakeh, and E. N. M. Quint, Phys. Lett. B **216**, 15 (1989).